High-spin binary black hole mergers

Pedro Marronetti,[1] Wolfgang Tichy,[1] Bernd Brügmann,[2] Jose González,[3, 2] and Ulrich Sperhake[2]

[1]*Department of Physics, Florida Atlantic University, Boca Raton, FL 33431, USA*
[2]*Theoretical Physics Institute, University of Jena, 07743 Jena, Germany*
[3]*Instituto de Física y Matemáticas, Universidad Michoacana de San Nicolás de Hidalgo, Morelia, Mexico*

We study identical mass black hole binaries with spins perpendicular to the binary's orbital plane. These binaries have individual spins ranging from $s/m^2 = -0.90$ to 0.90, ($s_1 = s_2$ in all cases) which is near the limit possible with standard Bowen-York puncture initial data. The extreme cases correspond to the largest initial spin simulations to date. Our results expand the parameter space covered by Rezzolla *et al.* and, when combining both data sets, we obtain estimations for the minimum and maximum values for the intrinsic angular momenta of the remnant of binary black hole mergers of $J/M^2 = 0.341 \pm 0.004$ and 0.951 ± 0.004 respectively. Note, however, that these values are reached through extrapolation to the singular cases $|s_1| = |s_2| = 1$ and thus remain as *estimates* until full-fledged numerical simulations provide confirmation.

I. INTRODUCTION

The existence of black holes, originally introduced as a family of solutions to the vacuum Einstein field equations, was a matter of speculation for the best part of the 20th century. In the past decade, however, astronomical observations placed them as the most promising models for objects detected in X-ray binaries (with sizes of a few to tens of solar masses) and for the supermassive entities at the center of some galaxies (with millions to billions of solar masses) [1]. Any black hole can be fully specified by its mass, angular momentum and charge. Since electrically charged black holes are quickly neutralized by free charges found in their vicinity (i.e, from accretion disks, interstellar plasma, etc.), only their mass and angular momentum are of astrophysical relevance. In a dynamical environment, several factors can determine the black hole's angular momentum: the characteristics of its progenitor (in case of stellar collapse formation), the merger with other black holes and neutron stars of comparable mass, the merger with smaller objects, and accretion of matter from a surrounding disk. (For a review on how these situations can alter the black hole rate of rotation and the bounds for the maximum spin attainable see, for instance, [2] and references therein.) Highly spinning black hole binaries are of particular interest given their astrophysical relevance. X-ray spectroscopic studies of accretion disks around the supermassive galactic black holes may provide evidence of spin parameters larger than 0.9 [3] (however, see for instance [4] on how this may only be a tentative estimate).

Recent progress in numerical relativistic simulations of binary black holes (BBH) [5, 6, 7] makes now possible long and stable evolutions that were impractical a few years ago. In this paper, we studied identical black holes with spins perpendicular to the orbital plane. In general, black hole spins would have arbitrary directions. However, it has been recently suggested [8] that supermassive galactic BBH may favor configurations with spin alignments like the ones studied here, due to the dynamical interaction of the holes with their galactic environments. Several groups have recently studied BBH with spins perpendicular to the orbital plane [9, 10, 11, 12, 13]. Here, we extend those studies, with binaries with initial individual spins ranging from $s/m^2 = -0.90$ to 0.90 (these extreme values are the largest modeled to date) with $m_1 = m_2$ and $s_1 = s_2$. The binaries in this sequence have not been considered before in such detail. Note also that, due to the symmetry of these systems, no gravitational recoil is present in the merger remnant.

We perform a least-square data fit of our data following the quadratic formula used by Campanelli *et al.* [9] and Rezzolla *et al.* [13] and also of both Rezzolla *et al.* and our data sets combined. The last fit predicts minimum and maximum values for the spin parameter of the black hole remnant of 0.341 ± 0.004 and 0.951 ± 0.004 respectively.

We find that current numerical techniques for the evolution of black holes with spins $s/m^2 > 0.75$ are limited in that they produce an artificial loss of angular momentum that increases with the magnitude of the spin. While this effect can be diminished by increasing the grid resolution, even relatively large resolutions such as $M/85$ present loss rates larger than 1% per $100M$ for the case $s/m^2 = 0.90$. This effect is clearly seen in the long term evolution of BBH that results in a highly spinning black hole and also on single black hole simulations.

In Sec. II, we present the numerical details and tests of our simulations. Sections III and IV present our results and conclusions.

II. NUMERICAL TECHNIQUES AND TESTS

All the binary systems studied here consist of identical black holes with spins aligned with the orbital angular momentum. In our coordinates, the orbit develops in the xy plane and the only non-vanishing component of the spins is in the $\hat{z}$ direction. We simulated binaries with spin parameters ranging from $s/m^2 = -0.90$ to 0.90.

As starting points of our simulations, we use stan-

s/m^2	m/M	m_b/M	D/M	P/M	M_i/M	J_i/M^2
-0.90	0.5000	0.1767	6.6965	0.14162	0.989	0.498
-0.75	0.5000	0.3307	6.6372	0.14041	0.988	0.557
-0.50	0.5000	0.4246	6.5366	0.13838	0.987	0.655
-0.25	0.5000	0.4656	6.4337	0.13631	0.986	0.752
0.00	0.5000	0.4777	6.3286	0.13419	0.986	0.849
0.25	0.5000	0.4654	6.2212	0.13204	0.985	0.940
0.50	0.5000	0.4240	6.1117	0.12983	0.985	1.043
0.62	0.5000	0.3888	6.0583	0.12875	0.985	1.090
0.75	0.5000	0.3299	6.0000	0.12756	0.985	1.140
0.82	0.5000	0.2810	5.9684	0.12691	0.985	1.167
0.90	0.5000	0.1764	5.9320	0.12616	0.985	1.198

TABLE I: Initial data parameters. Here m_b is the bare mass parameter of each puncture and $M = 2m$ is the sum of the ADM masses m measured at each puncture. The holes have coordinate separation D, with puncture locations $(0, \pm D/2, 0)$, linear momenta $(\mp P, 0, 0)$, and spins $(0, 0, s)$. We also list the initial values of the ADM mass M_i and the angular momentum J_i. The 2PN angular velocity is set to $\Omega M = 0.05550$ in each case.

dard puncture initial data [14] with the momentum and spin parameters in the extrinsic curvature given by second-order post-Newtonian (2PN) estimates [15]. It is sufficient to use 2PN estimates because standard puncture data are inconsistent with PN theory beyond $(v/c)^3$ [16, 17, 18, 19]. These parameters along with the initial ADM mass M_i and angular momentum J_i are shown in Table I. The coordinate distance D, the linear momenta P and spin parameters s are directly used in the Bowen-York extrinsic curvature, while the bare mass parameter is obtained from the condition that the ADM masses measured at each puncture should be $m = M/2$. As in [20, 21, 22] we assume that m is a good approximation for the initial individual black hole masses.

To complete the definition of the initial data, we also need to specify initial values for the lapse α and shift vector β^i. At time $t = 0$ we use

$$\alpha = \left(1 + \frac{m_b}{4r_1} + \frac{m_b}{4r_2}\right)^{-4},$$
$$\beta^i = 0,$$

where r_A is the coordinate distance from puncture A. Lapse and shift evolve according to

$$(\partial_t - \beta^i \partial_i)\alpha = -2\alpha K,$$
$$(\partial_t - \beta^k \partial_k)\beta^i = \frac{3}{4}B^i,$$
$$(\partial_t - \beta^k \partial_k)B^i = (\partial_t - \beta^k \partial_k)\tilde{\Gamma}^i - \eta B^i.$$

The gravitational fields are evolved using the "moving punctures" method [6, 7] with the implementation discussed in [23, 24], with the exception that as in [25] the dynamical variable ϕ has been replaced by the variable

$$W = e^{-2\phi},$$

Grid	Structure
1	$[5 \times 48 : 5 \times 54]$ $[h_{min} = M/56.9 : OB = 238.5M]$
2	$[5 \times 56 : 5 \times 63]$ $[h_{min} = M/66.4 : OB = 235.3M]$
3	$[5 \times 64 : 5 \times 72]$ $[h_{min} = M/75.9 : OB = 246.4M]$
4	$[5 \times 72 : 5 \times 81]$ $[h_{min} = M/85.3 : OB = 243.0M]$
5	$[5 \times 80 : 5 \times 90]$ $[h_{min} = M/94.8 : OB = 240.3M]$
6	$[5 \times 80 : 5 \times 90]$ $[h_{min} = M/85.3 : OB = 267.0M]$
L	$[3 \times 69 : 6 \times 149]$ $[h_{min} = M/80.0 : OB = 256.0M]$

TABLE II: Characteristics of our numerical grids. The values between brackets show the number of inner (moving) levels times the number of grid points per level per dimension, plus the number of outer (fixed) levels times the number of grid points. h_{min} is the finest grid spacing and OB gives the coordinate distance to the grid's outer boundary. The last entry corresponds to a grid used with the code LEAN [26].

which obeys the evolution equation

$$\partial_t W = \frac{1}{3}W\left(\alpha K - \partial_i \beta^i\right) + \beta^i \partial_i W.$$

The new variable W has two advantages. First, our simulations seem to converge better when we use W instead of ϕ or $\chi = e^{-4\phi}$ [6]. This may be related to the fact that W grows linearly near the black hole centers after some time of evolving the system. Such linear behavior leads to more accurate finite differencing derivatives near the punctures. In addition, the determinant of the 3-metric $\det(\gamma_{ij}) = W^{-6}$ remains always positive, even if W becomes slightly negative due to numerical error. This property is not ensured if one evolves, for example, the variable χ. In the latter case one has to explicitly guard against this to prevent code crashes.

The simulations presented here were performed using the BAM code, details of which are described in [23, 27]. BAM is based on three-dimensional Cartesian coordinates and can achieve high spatial resolution near the punctures using a structure of nested refinement levels. The outermost of these levels are fixed, while the innermost track the movement of the punctures. For the runs presented here, we used 10 levels of refinement with the outer boundaries located about $240M$ away from the grid center. Since the black holes are identical, we use quadrant symmetry. Table II lists the characteristics of the different grid layouts used in this paper. BAM characteristics make it ideal for quick and relatively inexpensive runs [24]. Most of the simulations presented here were done on dual processor workstations with characteristics speeds of 0.9, 1.7 and 2.5 days per orbit when using grids 1, 2 and 3 respectively.

Table III enumerates the binary simulations using the nomenclature SXX_Y, where XX indicates the value of s/m^2 and Y indicates which one of the numerical grids of Table II was used. We measure the mass and angular momentum of the remnant of the binary black hole merger using techniques based on volume integrals (see [24] for details). These values of mass and angular momentum are labeled M_f and J_f respectively.

Run	M_f/M	J_f/M^2	J_f/M_f^2
$S-0.90\_1$	0.976	0.348	0.365
$S-0.90\_2$	0.970	0.359	0.382
$S-0.90\_3$	0.970	0.358	0.380
$S-0.90\_4$	0.970	0.358	0.380
$S-0.75\_1$	0.970	0.405	0.431
$S-0.75\_2$	0.968	0.408	0.436
$S-0.75\_3$	0.968	0.409	0.437
$S-0.50\_1$	0.963	0.483	0.520
$S-0.50\_2$	0.963	0.486	0.524
$S-0.25\_1$	0.958	0.551	0.600
$S-0.25\_2$	0.958	0.555	0.606
$S+0.00\_1$	0.951	0.605	0.669
$S+0.00\_2$	0.951	0.614	0.679
$S+0.00\_3$	0.951	0.619	0.684
$S+0.00\_4$	0.951	0.619	0.684
$S+0.25\_1$	0.944	0.671	0.753
$S+0.25\_2$	0.944	0.676	0.759
$S+0.50\_1$	0.934	0.721	0.827
$S+0.50\_2$	0.933	0.720	0.826
$S+0.62\_1$	0.927	0.731	0.851
$S+0.62\_2$	0.926	0.737	0.859
$S+0.62\_3$	0.926	0.737	0.859
$S+0.75\_1$	0.917	0.729	0.866
$S+0.75\_2$	0.916	0.733	0.874
$S+0.75\_3$	0.916	0.736	0.877
$S+0.75\_4$	0.916	0.738	0.880
$S+0.82\_1$	0.911	0.688	0.828
$S+0.82\_2$	0.910	0.703	0.850
$S+0.82\_3$	0.909	0.701	0.848
$S+0.90\_1$	0.905	0.645	0.788
$S+0.90\_2$	0.905	0.640	0.781
$S+0.90\_3$	0.903	0.643	0.788
$S+0.90\_4$	0.902	0.643	0.790
$S+0.90\_5$	0.902	0.646	0.794
$S+0.90\_6$	0.906	0.644	0.785

TABLE III: Binary black hole simulations performed for this paper. The runs are named SXX_Y, where XX indicates the value of s/m^2 and Y is the numerical grid used for that run. Table II describes the different grids.

We study the effect of different approximations and limitations inherent to our simulations: grid resolution, grid structure, measurement of the final mass and angular momentum, and the intrinsic characteristics of our initial data sets. We start by varying the spatial resolution of our grids, while keeping the grid size and structure (i.e., the layout of the refinement levels) unchanged. Grids 1 to 5 cover maximum spatial resolutions going from $M/56.9$ to $M/94.8$. The results, presented in Table III, do not seem to vary significantly with the spatial resolution: the values of J_f/M_f^2 obtained for grids 2 to 5 agree with each other at a level of about 1.5% or better. We test the convergence of the calculations of mass and angular momentum, using four runs for the binary with spin $s/m^2 = 0.90$ (labeled $S+0.90\_Y$, Y=1 to 4). These runs shared the same grid layout but with vary-
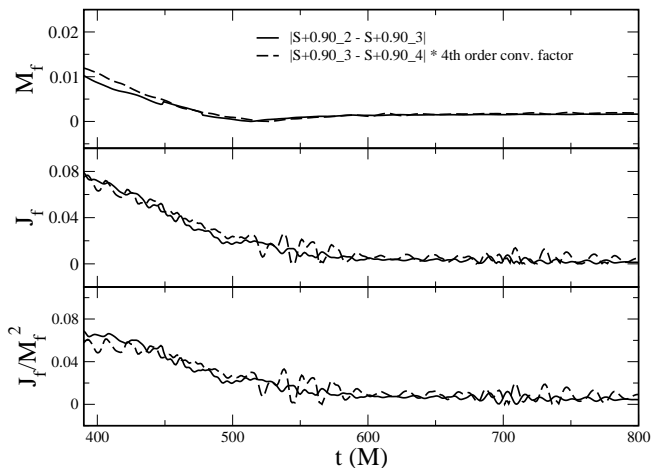

FIG. 1: Mass and angular momentum plots for three different resolutions. The dashed curves have been scaled according to a factor corresponding to 4th order convergence in spatial resolution.

ing spatial resolution, ranging from $h_{min} = M/56.9$ to $h_{min} = M/85.3$ [36]. We find that the lowest resolution run ($S+0.90\_1$) fell outside the convergence regime. The results of the other three runs, presented in Fig. 1, seem to show that these runs are in the convergent regime.

To evaluate the influence of the grid layout, we compare the results from two grids with identical resolution but different number of grid points per box (Grids 4 and 6 from Table II). The box size has been found crucial in previous work [23]: boxes smaller than critical sizes tend to change drastically the binary dynamics, altering orbits and merger times. Runs $S+0.90\_4$ and $S+0.90\_6$ returned values of mass and angular momentum with differences of $\Delta M_f = 4\ 10^{-3}(0.4\%)$ and $\Delta J_f = 5\ 10^{-4}(0.1\%)$ respectively.

Additionally, and as an independent check, we compare our results with those of Campanelli *et al.* [28] (shown in Fig. 2 as empty circles) and Pollney *et al.* [12] (empty square).

To evaluate the accuracy of the algorithms used to measure mass and angular momentum, we compare our volume-integral based results with calculations done using surface integrals [24] and find differences of up to 0.5% in magnitude. We also test the satisfaction of the Christodoulou formula $J_c = 2\ M_{irr}\ (M_f^2 - M_{irr}^2)^{1/2}$ (M_{irr} being the irreducible mass of the final black hole). The relative difference in the values of J_f and J_c for the run $S+0.90\_5$ was less than 0.5%.

III.   RESULTS

Figure 2 summarizes the results of Table III. The spin parameter of the binary remnant J_f/M_f^2 is shown as a function of the initial black hole spins s/m^2. These values were measured at $500M$ after the merger (which cor-
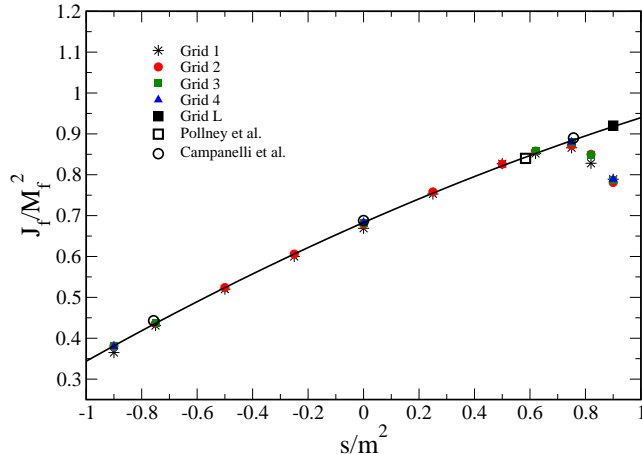
FIG. 2: Spin of the merger remnant as a function of the initial black hole spins measured $500M$ after the black hole merger. The binaries are composed of identical black holes with initial spins of magnitude s/m^2 aligned with the orbital angular. The values calculated in [28] ([12]) are shown as empty circles (square). The solid square represents the remnant spin calculated right after the merger for the case $s/m^2 = 0.90$, using Grid L. The solid line is a quadratic interpolation of the values corresponding to Grid 2 for $s/m^2 < 0.75$ plus the Grid L value.
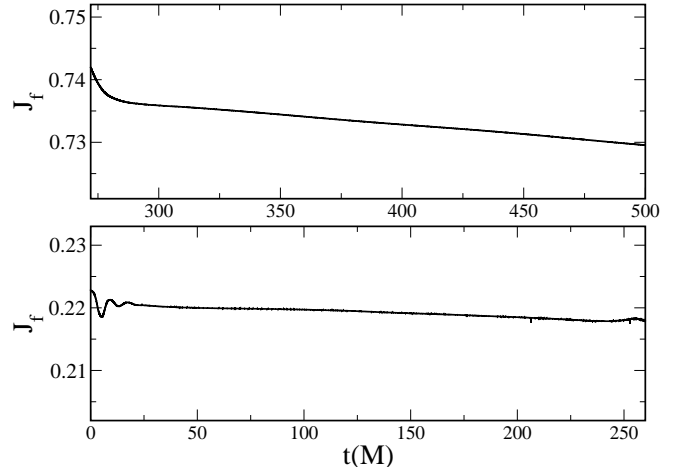
FIG. 3: Evolution of the angular momentum for the binary with $s/m^2 = 0.90$ obtained using the isolated horizon techniques of [9]. The top plot corresponds to the angular momentum of the remnant of the merger, while the bottom plot tracks the spin of the individual black holes before the merger (occurring at $265M$).

responds approximately to the side-to-side light-crossing time of our grids). The most striking feature of the plot is the existence of an apparent maximum at $s/m^2 \approx 0.75$. As we will see, this maximum is merely a numerical artifact caused by an artificial loss of angular momentum in the case of highly spinning black holes if we wait for $500M$ after the merger. Shortly after the merger, the spin of the remaining black hole is still larger. This is confirmed by a simulation of the $s/m^2 = 0.90$ case using the LEAN code (Grid L in Table II) that tracks the common apparent horizon and the emission of energy and angular momentum in the form of gravitational waves. We calculate the spin about $50M$ after the merger in four different ways: from the balance of gravitational wave energy and angular momentum loss, from the ringdown frequencies (using the tabulated results given in [29]), from the isolated horizon geometry (using the techniques from [9]), and using Christodoulou's formula. The corresponding results are $J_f/M_f^2 = 0.95$, 0.925, 0.913, 0.918 respectively. The first result is the least accurate, given that the wave extraction radius ($50M$) was not considerably far from the center. The rest cluster around 0.92 (plotted in Fig. 2 as a solid square) that agrees better with an extrapolation from lower s/m^2 results. Figure 3 shows the evolution of the angular momentum obtained using isolated horizon techniques which indicates a loss rate of about 0.5% per $100M$. This last result together with the measurements at $500M$ after the merger seem to indi-

cate an artificial loss in angular momentum for high spin black holes. Also note that this effect is not seen at the lower spin end of Fig. 2. This is simply due to the fact that the merger remnant of binaries with individual spins $s/m^2 < 0.75$ is a low spinning black hole, and thus not affected by this effect.

To study this effect in more detail, we perform single black hole evolutions. Figure 4 compares evolutions for the cases with $s/m^2 = 0.53$ and 0.90. In order to facilitate the comparison, we plot the relative differences from the initial values of the mass, angular momentum and intrinsic angular momentum parameter, these quantities measured using volume integrals methods. The angular momentum loss, while negligible in the 0.53 case, is more pronounced in the larger spin case. Note however that the mass is largely unaffected in both cases. Figure 5 shows the results for four different grid resolutions, indicating firstly that the mass is better conserved than the angular momentum and secondly that this loss gets smaller with increasing resolution, albeit quite slowly. The angular momentum curves are still consistent with 4th order convergence, however, Richardson extrapolating these curves to arbitraily large resolution still shows loss of angular momentum. For BBH evolutions with many orbits before the merger, this loss could in principle produce an "effective" value of s/m^2 at the time of the merger smaller than the initially intended. In order to evaluate this effect, we track the evolution of the individual spins before the merger as shown in the bottom panel of Fig. 3. An angular momentum loss of about 3% is detected before the merger, which occurs at $t = 265M$.
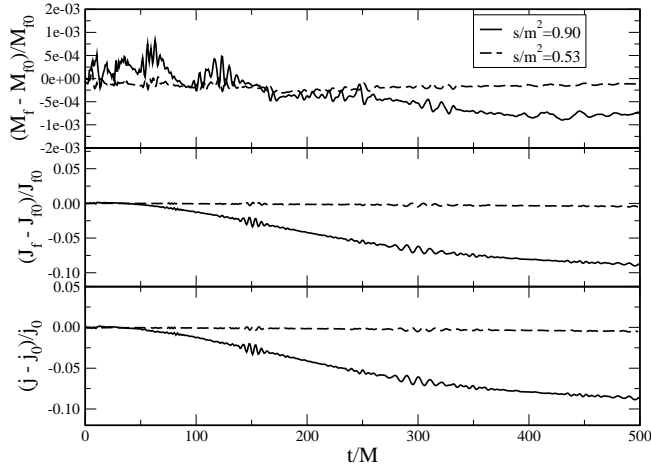
FIG. 4: Single black hole evolutions with $s/m^2 = 0.53$ (dashed) and 0.90 (solid), on Grid 4. The plots present the relative differences with respect to the initial values, denoted with the 0 sub-index. The bottom plot presents the relative variation of intrinsic angular momentum $j \equiv J_f/M_f^2$.
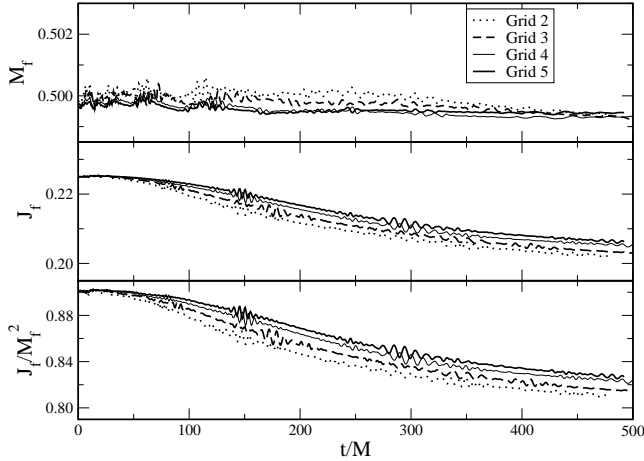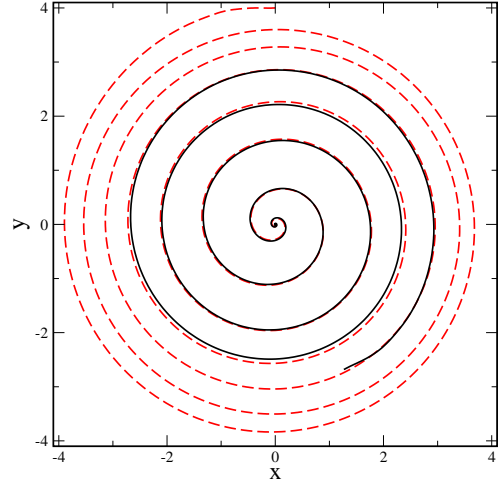

FIG. 6: Puncture tracks of one of the holes for two simulations with $s/m^2 = 0.90$ that start out at different coordinate separations; $D = 8M$ (dashed) and $D = 6M$ (solid). The $D = 6M$ orbits have been rotated to coincide with the ones from the $D = 8M$ case in the final orbits. Both runs were performed using Grid 3.

FIG. 5: Evolution of single black holes with $s/m^2 = 0.90$ for different spatial resolutions.

At first sight, part of this loss could also be attributed to our choice of initial data. Traditionally, puncture initial data sets are constructed by solving the Hamiltonian constraint under the assumption of conformal flatness for the spatial metric. The momentum constraint is analytically satisfied by the use of the Bowen-York (BY) formula for the extrinsic curvature which, in principle, allows for the arbitrary specification of the linear and angular momentum of the black holes. In practice, the amount of

"junk radiation" associated with these initial data sets increases with the magnitude of the spin of the hole. The amount of this extra radiation has been studied perturbatively by Gleiser $et\ al.$ [30] and numerically by Hannam $et\ al.$ [31] and Dain $et\ al.$ [32]. The last shows that, for the case $s/m^2 = 0.90$, a single BY black hole would relax into a Kerr black hole after emitting about 0.1% of the initial gravitational mass.

To further study this effect in the evolution prior to the merger, we perform a simulation of a binary with $s/m^2 = 0.90$ that starts out at a coordinate separation $D = 8M$ and compare it with one starting at $D = 6M$. The former simulation lasted more than two orbits and a half longer than the latter, corresponding to an additional simulation time of $395M$. Figure 6 shows the orbits of one of the punctures for these simulations. Both runs were performed using Grid 3. Figure 7 shows the corresponding evolution of the mass and angular momentum, where the curves corresponding to the $D = 8M$ run were shifted in time by $395M$. Naively, one would expect the $D = 8M$ to dissipate more angular momentum before the merger, given that it is more than two orbits longer than its $D = 6M$ counterpart. This would result in the longer run remnant having a smaller intrinsic spin than the shorter evolution. However, the resulting spin for the $D = 8M$ run is about 3% larger for the $D = 6M$ case, but within the error margin for these measurements, making it difficult to draw any conclusions.

Next, we fit the values of the highest resolution runs from Table III, ignoring the results for $s/m^2 > 0.75$, but adding the result at $s/m^2 = 0.90$ from Grid L (solid
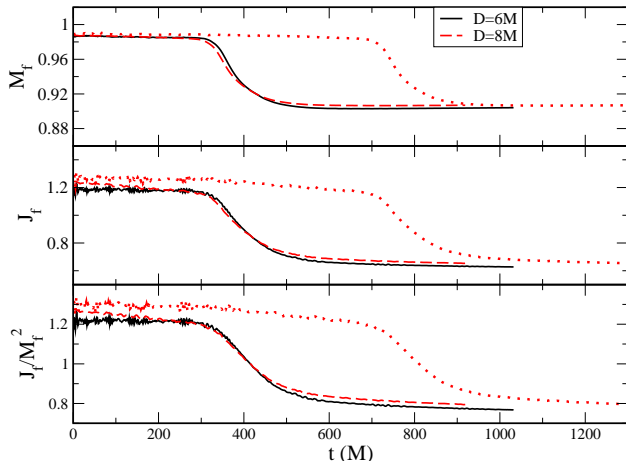
FIG. 7: Evolution of mass and angular momentum for the runs of Fig. 6. The solid (dotted) lines corresponds to the separation $D = 6M$ ($D = 8M$). The dashed line corresponds to the $D = 8M$ run shifted in time by $395M$.

	C	R	M	R+M
p_0	0.6879	0.6883(4)	0.6855(16)	0.6888(4)
p_1	0.1476	0.1530(4)	0.1499(8)	0.1525(5)
p_2	-0.0093	-0.0088(5)	-0.0110(8)	-0.0106(5)
Max J/M^2	0.946	0.959(2)	0.941(6)	0.951(4)
Min J/M^2	0.355	0.347(2)	0.342(6)	0.341(4)

TABLE IV: Least-squares fit of Eq. (1) from Campanelli *et al.* [9] (**C**), Rezzolla *et al.* [13] (**R**), this paper (**M**), and Rezzolla *et al.* and our data sets combined (**R+M**). The last two rows show the extrapolation to initial critical black holes aligned (counter-aligned) with the orbital angular momentum that corresponds to the maximum (minimum) possible intrinsic spin for the remnant black hole.

square). We follow the fitting formula for the final black hole intrinsic spin used in Campanelli *et al.* [9] and Rezzolla *et al.* [13] (Eq. (8))

$$
\begin{aligned}
J_f/M_f^2 = p_0 \; + \; & p_1 \, (s_1/m_1^2 + s_2/m_2^2) \\
& + \; p_2 \, (s_1/m_1^2 + s_2/m_2^2)^2,
\end{aligned} \tag{1}
$$

where p_0, p_1 and p_2 are the fitting parameters. We present in Table IV a comparison of our best fit parameters with those from [9] and [13] and with the ones obtained by fitting [13] and our data sets together. For these fits, we assume a nominal error of 0.02 for all our values. We see that the fitting parameters are in an agreement consistent with small-number statistics in all cases. Table IV also shows the extrapolation to maximally rotating black holes, aligned and counter-aligned with the orbital angular momentum. The maximum and minimum values for the intrinsic angular momentum of the

remnant predicted by the fit of the combined data sets is $J_f/M_f^2 = 0.341 \pm 0.004$ and 0.951 ± 0.004 respectively [37]. Note that, while our data set is smaller than the one in [13], it contains measurements that are closer to the extrapolated values for critical BBH.

Recently, Boyle *et al.* [33] introduced a formalism that predicts any final quantity resulting from the merger using a Taylor expansion on the initial binary mass ratio $q \equiv m_1/m_2$ and the components of the initial spins. For the highly symmetric binaries considered in this paper, their expansion for J_f/M_f^2 to second order reduces to the polynomial of Eq. (1) with the equivalences $p_0 = s_3^{000|000}$, $p_1 = s_3^{001|000}$ and $p_2 = (1/4) \, (2 \, s_3^{002|000} + s_3^{001|001})$, where the parameters on the right-hand sides are those from the corresponding expansion in [33].

Finally, we would like to highlight the ability of the code BAM to probe accurately and efficiently BBH parameter space. Our lowest resolution runs (Grid 1), performed on dual-processor workstations, are good enough to capture the main characteristics of the results of Fig. 2.

IV. CONCLUSIONS

We studied the effect of the initial spins of the black holes in a binary system on the mass and angular momentum of the black hole that results from the merger. We concentrated on equal-mass binaries with spins aligned with the orbital angular momentum ($s_1 = s_2$), covering a range of initial spin parameters going from $s/m^2 = -0.90$ to 0.90. The runs at the extrema of the range are the highest spin simulations to date. The main results of the paper are presented in Fig. 2, where the spin parameter of the remnant (J_f/M_f^2) is given as a function of the initial spin parameters.

We combined our results with those of Rezzolla *et al.* [13] in a quadratic least-square fit and obtain, by extrapolation to initial critical black holes, predicted maximum and minimum values of J/M^2 for the black hole remnant of 0.951 ± 0.004 and 0.341 ± 0.004 respectively. These error bounds are simply derived from the uncertainty of the fitting parameters provided by their standard error. The small size of the samples studied here plus the fact that the limits to critical black hole results are obtained through extrapolation to points in parameter space with singular properties may lead to revisions in these estimates once binaries with spins larger than 0.90 can be accurately simulated. For this, new recipes for initial data sets that allow for initial black holes with spin parameters larger than 0.928 (the limit of BY data) are needed. The methods introduced by Dain [34, 35] and studied in head-on BBH simulations by Hannam *et al.* [31] may hold the key to this problem.

We also find a problem for the simulations starting with spins $s/m^2 > 0.75$. Current evolutions based on the moving punctures methods present losses of angular

momentum at non-negligible rates for highly spinning black holes, even when relatively high grid resolutions are employed. Measurements of the merger remnant intrinsic spin $500M$ after the merger of two $s/m^2 = 0.90$ black holes show the spurious loss of more than 10% of the angular momentum. This effect increases with the magnitude of the black hole spin. This loss does not affect strongly the calculation of gravitational wave templates, since they cover only up to a short period after the merger. However, it becomes more important, for instance, for simulations of black hole-neutron star or neutron star-neutron star binaries, where the potential formation of an accretion disk around a black hole has to be followed for much longer periods.

Acknowledgments

[1] R. Narayan, New J. Phys. **7**, 199 (2005), gr-qc/0506078.
[2] C. F. Gammie, S. L. Shapiro, and J. C. McKinney, Astrophys. J. **602**, 312 (2004), astro-ph/0310886.
[3] C. S. Reynolds, L. W. Brenneman, and D. Garofalo, Astrophys. Space Sci. **300**, 71 (2005), astro-ph/0410116.
[4] K. Nandra, P. M. O'Neill, I. M. George, J. N. Reeves, and T. J. Turner, Astron. Nachr. **327**, 1039 (2006), astro-ph/0610585.
[5] F. Pretorius, Phys. Rev. Lett. **95**, 121101 (2005), gr-qc/0507014.
[6] M. Campanelli, C. O. Lousto, P. Marronetti, and Y. Zlochower, Phys. Rev. Lett. **96**, 111101 (2006), gr-qc/0511048.
[7] J. G. Baker, J. Centrella, D.-I. Choi, M. Koppitz, and J. van Meter, Phys. Rev. Lett. **96**, 111102 (2006), gr-qc/0511103.
[8] T. Bogdanovic, C. S. Reynolds, and M. C. Miller, Ap. J. Lett. **661**, L147 (2007), astro-ph/0703054.
[9] M. Campanelli, C. O. Lousto, Y. Zlochower, B. Krishnan, and D. Merritt, Phys. Rev. **D75**, 064030 (2007), gr-qc/0612076.
[10] F. Herrmann, I. Hinder, D. Shoemaker, P. Laguna, and R. A. Matzner, Phys. Rev. D **76**, 084032 (2007), arXiv:0706.2541.
[11] M. Koppitz, D. Pollney, C. Reisswig, L. Rezzolla, J. Thornburg, P. Diener, and E. Schnetter, Phys. Rev. Lett. **99**, 041102 (2007), gr-qc/0701163.
[12] D. Pollney, C. Reisswig, L. Rezolla, B. Szilagyi, M. Ansorg, B. Deris, P. Diener, E. Dorband, M. Koppitz, A. Nagar, et al., Phys. Rev. D **76**, 124002 (2007), arXiv:0707.2559.
[13] E. L. Rezzolla, N. Dorband, C. Reisswig, P. Diener, D. Pollney, E. Schnetter, and B. Szilagyi (2007), arXiv:0708.3999.
[14] S. Brandt and B. Brügmann, Phys. Rev. Lett. **78**, 3606 (1997), gr-qc/9703066.
[15] L. E. Kidder, Phys. Rev. **D52**, 821 (1995), gr-qc/9506022.
[16] W. Tichy, B. Brügmann, M. Campanelli, and P. Diener, Phys. Rev. D **67**, 064008 (2003), gr-qc/0207011.
[17] N. Yunes and W. Tichy, Phys. Rev. D **74**, 064013 (2006), gr-qc/0601046.
[18] N. Yunes, W. Tichy, B. J. Owen, and B. Bruegmann, Phys. Rev. D **74**, 104011 (2006), gr-qc/0503011.
[19] B. J. Kelly, W. Tichy, M. Campanelli, and B. F. Whiting, Phys. Rev. **D76**, 024008 (2007), arXiv:0704.0628.
[20] W. Tichy, B. Brügmann, and P. Laguna, Phys. Rev. D **68**, 064008 (2003), gr-qc/0306020.
[21] W. Tichy and B. Brügmann, Phys. Rev. D **69**, 024006 (2004), gr-qc/0307027.
[22] M. Ansorg, B. Brügmann, and W. Tichy, Phys. Rev. D **70**, 064011 (2004), gr-qc/0404056.
[23] B. Brügmann, J. Gonzalez, M. Hannam, S. Husa, U. Sperhake, and W. Tichy, Phys. Rev. D **77**, 024027 (2008), gr-qc/0610128.
[24] P. Marronetti, W. Tichy, B. Bruegmann, J. Gonzalez, M. Hannam, S. Husa, and U. Sperhake, Class. Quantum Grav. **24**, S34 (2007), gr-qc/0701123.
[25] W. Tichy and P. Marronetti, Phys. Rev. D **76**, 061502 (2007), arXiv:gr-qc/0703075.
[26] U. Sperhake, Phys. Rev. D **76**, 104015 (2007), gr-qc/0606079.
[27] B. Brügmann, W. Tichy, and N. Jansen, Phys. Rev. Lett. **92**, 211101 (2004), gr-qc/0312112.
[28] M. Campanelli, C. O. Lousto, and Y. Zlochower, Phys. Rev. D **74**, 041501 (2006), gr-qc/0604012.
[29] E. Berti, V. Cardoso, and C. M. Will, Phys. Rev. D **73**, 064030 (2006), gr-qc/0512160.
[30] R. J. Gleiser, C. O. Nicasio, R. H. Price, and J. Pullin, Phys. Rev.D **57**, 3401 (1998).
[31] M. Hannam, S. Husa, B. Brügmann, J. A. Gonzalez, and U. Sperhake, Class. Quant. Grav. **24**, S15 (2007), gr-qc/0612001.
[32] S. Dain, C. O. Lousto, and R. Takahashi, Phys. Rev. D

65, 104038 (2002), gr-qc/0201062.

[33] L. Boyle, M. Kesden, and S. Nissanke (2007), arXiv:0709.0299.

[34] S. Dain, Phys. Rev. Lett. **87**, 121102 (2001), gr-qc/0012023.

[35] S. Dain, Phys. Rev. D **64** (2001), gr-qc/0103030.

[36] Run S+0.90_5 was not used because the high order of our algorithms (fourth) made the difference in results fall too close to our calculation round-off error for meaningful convergence tests.

[37] To asses the influence of the LEAN data point in our results, we re-calculated our predictions for the maximum and minimum values of J_f/M_f^2 without it. The new results are within the error bands of the values quoted in Table IV